RPE | Radiation Physics & Engineering
A Peer-Reviewed Journal
Published by K.N. Toosi University of Technology
http://rpe.kntu.ac.ir
Research Article

Radiation Physics and Engineering 2025; 6(3):27–33

Feasibility study of dual-energy limited-number-detector computed tomography of oil and gas pipelines

Mostafa Kabir[a], Hossein Afarideh[a,*], Mitra Ghergherehchi[b], Jong-Seo Chai[b]

[a] *Department of Energy Engineering and Physics, Amirkabir University of Technology (Tehran Polytechnic), Tehran, Iran*
[b] *Department of Electrical and Computer Engineering, Sungkyunkwan University, Suwon, South Korea*

HIGHLIGHTS

- Dual-energy technique for contrast enhancement of pipeline computed tomography.
- Proactive pipeline condition monitoring with dual-energy LNDCT offers significant advantages.
- Monte Carlo simulations were employed to optimize the dual-energy LNDCT system.
- Innovative limited-number-detector computed tomography (LNDCT) technology was applied for image formation.

ABSTRACT

Fluid transmission pipelines are prone to corrosion and sediment deposition due to the nature of the materials they carry. Deposits inside of the pipeline may worsen corrosion, leading to micro-cracks and pitting. Neglecting to assess these factors can lead pipelines to failures with catastrophic consequences. Therefore, monitoring and measuring corrosion, erosion, and sedimentation levels within pipelines are crucial. Various methods have been developed for this purpose, with techniques using penetrating X-rays and gamma rays being the most accurate and non-destructive. In this study, gamma-ray dual-energy computed-tomography was utilized as a precise and non-destructive method for detecting corrosion in pipeline walls. Projections were obtained using the Limited-Number-Detector Computed Tomography (LNDCT) technique for pipeline phantoms. Dual-energy techniques were employed, emitting gamma rays from suitable radioactive isotopes such using two radioisotopes, Am-241 and Cs-137. Projections at different angles were recorded using 15 NaI(Tl) 2-inch detectors, and the corresponding full-energy-peak were separated and organized in the sinogram matrix. Subsequently. Image reconstruction was performed using the Filtered-Back-Projection (FBP) algorithm, and the quality of the reconstructed image was assessed. The reconstructed images demonstrate the effectiveness of the dual-energy method in distinguishing between light and heavy materials, potentially leading to higher image quality compared to single-energy methods. Detailed analysis of the data obtained from dual-energy tomography enables precise identification of defects, failures, and sedimentation, without damages to pipeline structures. This research contributes to enhancing the evaluation and monitoring methods for pipelines, improving the efficiency of these systems, and ultimately advancing safety and productivity in the oil and gas industry.

KEYWORDS

Computed Tomography
Dual-energy technique
Pipelines Corrosion
Scale Measurement
NaI(Tl) detector

HISTORY

Received: 23 November 2024
Revised: 3 January 2025
Accepted: 9 January 2025
Published: Summer 2025

1 Introduction

In the oil, gas, and petrochemical industries, deposits and corrosion pose serious problems for pipeline transportation systems (Kamal et al., 2018; Zahedzadeh et al., 2014). Significant volumes of chemicals leak from pipelines every year as a result of corrosion, endangering the environment or causing pipeline explosions. Deposit formation in pipeline veins lowers fluid flow volume and speeds up erosion and corrosion, which causes further damage. A good way to gauge and quantify corrosion is to take a measurement of the pipeline wall's thickness. For this goal, a number of non-destructive techniques have been developed; gamma ray attenuation, also known as X-ray penetrating radiography, is one of the most successful (Harara, 2005; Rostron, 2018; Azaman et al., 2016; Prasetyo et al.,

*Corresponding author: hafarideh@aut.ac.ir

https://doi.org/10.22034/rpe.2025.490153.1257

2020; Zirnhelt et al., 2003; Oliveira et al., 2015). Gamma-ray tomography equipment has recently been available for cross-sectional imaging within pipelines. Kabir et al., introduced the limited-number-detector computed tomography (LNDCT) with a novel projection acquisition method (Kabir et al., 2024). With this method, silt thickness in pipelines may be measured without requiring shutdowns or discharge, giving pipeline system managers a proactive and accurate way to evaluate the condition of their pipes. These devices use 360-degree gamma-ray attenuation around the pipeline to produce projections, which are then followed by picture reconstruction (Kim et al., 2011). Nevertheless, these systems have a limited number of detectors, which results in less-than-ideal image quality. As a result, a lot of study has been done on ways to either enhance image quality or make up for missing detectors (Kim et al., 2011, 2012a,b; Khorsandi and Feghhi, 2016). Numerous studies have examined the use of Monte Carlo simulation for pipeline tomography parameter evaluation (Ay and Zaidi, 2005; Velo et al., 2017; Smith et al., 2022). The primary area of feasibility study in this research is dual-energy approaches, which can improve the performance of single-energy scanning devices, especially when working with nearby light and heavy materials like scales or the insulation surrounding oil and gas pipelines. To produce an image, common systems now in use only use one gamma-ray emitting source and one photopeak (Chung et al., 2023). Insufficient distinction is made between light and heavy elements in this kind of single energy tomographic image.

To enhance the most important image quality parameters like contrast and contrast-to-noise ratio and also having better analysis by discriminating materials lead us to propose and design dual-energy limited-number-detector feasibility study. In this way, this paper focused on the optimum design of and configuration to implement dual-energy LNDCT by a reliable approach of collecting low-energy (LE) and high-energy (HE) signals from detectors simultaneously. Monte-carlo simulation as a powerful tool was employed to study different aspects of dual-energy method for pipelines LNDCT.

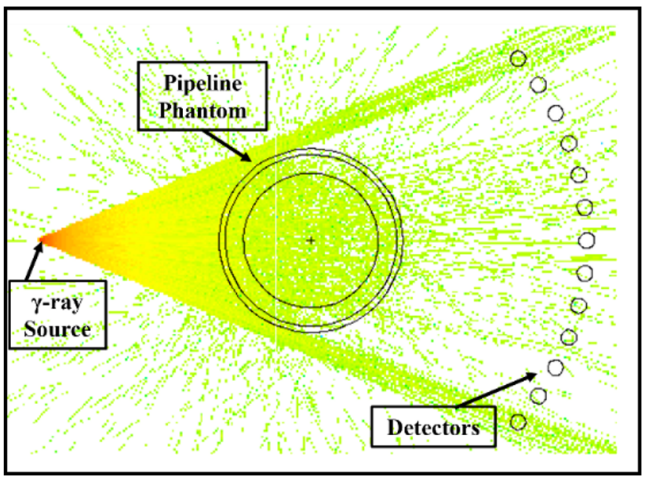

Figure 1: Gamma-ray photon transport through pipeline phantom.

2 Materials and Methods

2.1 Monte Carlo Modelling

One of the most precise techniques for modeling of ionized radiation and transporting high-energy photons intracting with matter and predicting radiative parameters is Monte Carlo (MC) simulation (Srinivas-Rao et al., 2023; Hartley-Blossom and Digumarthy, 2023). In a typical MC photon tracking code, gamma-ray photons at high and low energies are generated in source according to their different probabilities of emission. After traveling through the material, the photons reach the detector and are recorded and monte-carlo calculation terminates when a particle reaches to its energy or place cutt-off. The intensity (flux or fluence) of photons that enter the detector within the energy ranges given by the tally detectors is measured in order to calculate our interest radiation parameter such as flux, current, energy etc. (Böttcher et al., 2023).

It takes a lot of time to simulate the whole process of creating and running the 360-degree codes. As a result, a computer program was created to create the input files for the Monte Carlo code using a predefined template because of the huge number of inputs and high volume of outputs produced by the code. Following the execution of the programs for each angle, the results are kept apart in a folder. In the meantime, each detector's recorded data from the tally detectors is extracted of the outputs and saved as an angle-tagged matrix. The outputs at each angular position, corresponding to the measured projections, are sequentially concatenated to form the sinogram matrix, a two-dimensional representation of the projection data. This sinogram serves as a comprehensive dataset encompassing the spatial variations of the attenuated signal across all viewing angles. Once the sinogram is fully assembled, advanced reconstruction algorithms, such as filtered back-projection (FBP) or iterative techniques, are applied to transform the projection data into a detailed cross-sectional image of the internal structure. This reconstruction process effectively maps the attenuation coefficients, yielding a high-resolution tomographic image that provides insight into the material's internal composition. Figure 1 shows a visual transport of Cs-137 gamma-ray photons which pass through pipeline and recorded on detectors. The main components implemented in the code is gamma-ray emitter source Cs-137, test phantom of a carbon steel pipe and anhydrite scale deposited in there as defined in section 2.3 and 15 NaI(Tl) detectors places on the curve line exactly in front of detector field-of-view (FOV) and there is nothing between two adjacent detectors. The beam shape is controlled by source bias card to prevent unwanted MC calculation as a variance reduction. The monte-carlo calculation continued to reaching $> 5\%$ relative error.

The validation of our simulation was conducted through an experimental setup. Gamma-ray sources were positioned within a lead collimator that produces a fan-beam with a vertex angle of 40 degrees and a beam width of 3 mm. A two-inch NaI(Tl) sodium iodide detector was employed, encased in a lead shield to minimize background radiation and block scattered rays. The positioning and

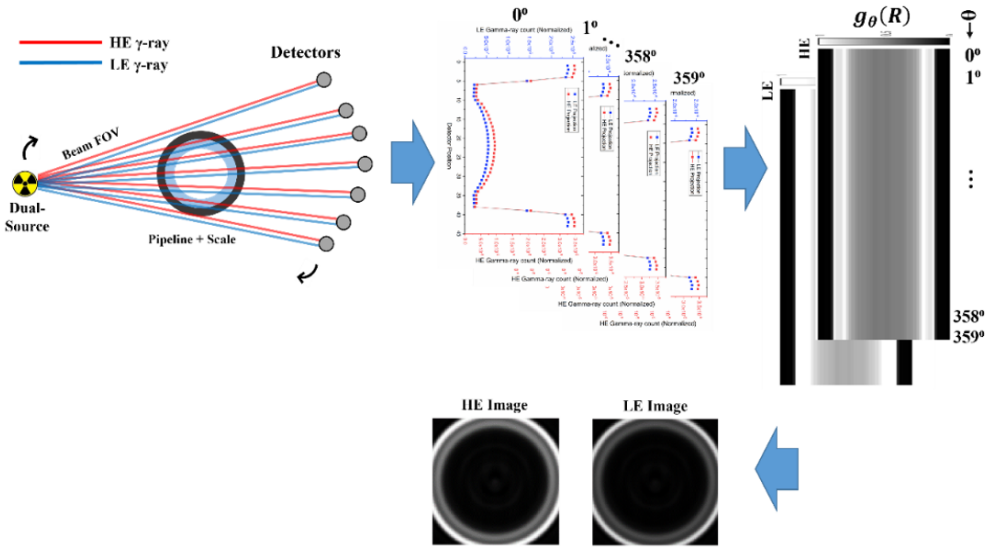

Figure 2: Schematic process from signal acquisition to image reconstruction for dual-energy LNDCT.

angular orientation of the sodium iodide cylindrical detector are configured such that radiation enters the detector exclusively through its flat surface, where pulse heights are recorded. Furthermore, the physical window for radiation entry is specifically designed and optimized to register and count only the radiation with a zero-degree angle (originating from photoelectric interactions). The experimental setup included two distinct phantoms: a 3 mm thick carbon steel pipeline and a 6 mm thick aluminum pipeline, both of which contained a hollow Teflon cylinder with a thickness of 2 cm.

2.2 Dual-Energy Method

Dual-energy (DE) gamma rays are released from the source and travel via a pipeline and any other medium in their course before reaching at detectors positioned on a curved trajectory and being recorded, as shown in Fig. 2. Data from all 15 detectors, which are 2 inch-sized NaI(Tl) detector, are recorded at each primary angle θ. The projections are then extracted around the pipeline using the energy separation module for high (HE) and low energies (LE) (Fig. 3). The sinogram matrix is then created by contrasting the projections that were acquired from the LE and HE signals. The filtered-back-projection analytical reconstruction algorithm is then used to reconstruct each matrix into a tomographic image, which is subsequently shown on the computer. Projection data acquisition is carried out by an automatic program. In the program using an input template of MC code in for example $\theta = 0°$, the other 359° input files will generate. Then each prepared code executes automatically one by one. The output file then readout by another computer program and projection data (tallies on detectors) will be extracted.

2.3 Test Phantom

Since pipeline tomography and evaluation are the ultimate uses for this approach, the following definition of a phantom was established: Phantom A: pipeline constructed of carbon steel with an outside diameter of 15 cm and a wall thickness of 3 mm. The scale deposits are composed of 1.2 cm thick $CaSO_4$ (anhydrite). The material characteristics of the test and evaluation phantom used in the Monte Carlo code are shown in Table 1.

2.4 Sources

Due of the higher relative density of the materials traversed by the radiation, Phantom was irradiated using two gamma emitter sources: Am-241 and Cs-137. Table 2 displays the energy specifications of the sources that were used. In this Monte-carlo feasibility study, the activity of the sources is not considered but the probability of emission is considered equal for both Cs-137 and Am-241 gamma ray sources. Am-241 source's gamma ray energy is about 60 keV which has low penetration power in materials. So, it used for thin pipeline wall or low atomic number materials like aluminum. The half-value-layer (HVL) for steel and aluminum are 3.35 cm and 0.415 cm respectively. Based on the typical standards, 10% of the photons reaching to the detector are acceptable. Considering the equal probabilities of gamma-ray emission from Cs-137 and Am-241 sources, in the Monte Carlo code, it is assumed that the sources have identical activity levels compared to the actual conditions.

Table 1: Material used in MC study.

Material	Density (g.cm^{-3})
Anhydrite (Calcium Sulphate)	2.80
Carbon Steel	7.82

Table 2: Gamma-ray emitter sources used in the feasibility study of the dual-energy method.

Radioisotope Source	Effective γ Energy (keV)	Probability (%)	Half-life (Years)
Cs-137	662	100%	30.2
Am-241	59.5	100%	432

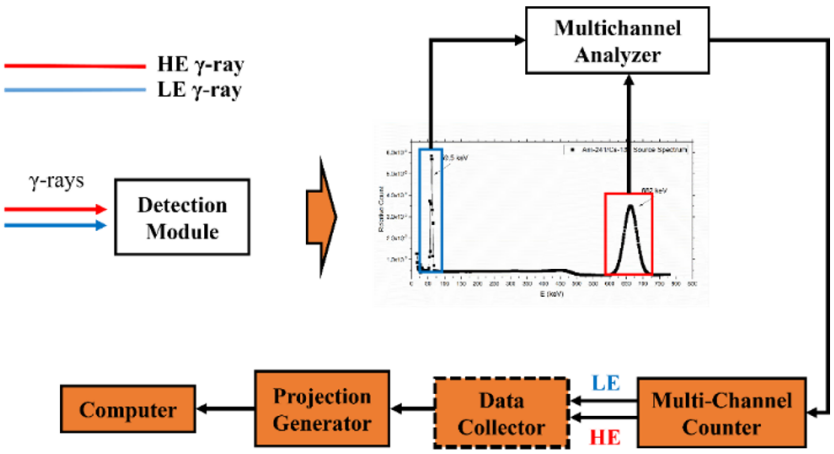

Figure 3: Schematic of discrimination process of LE and HE signals to generate projections at each angle θ_i.

2.5 Signal Separation

NaI(Tl) detectors, which offer good energy discrimination capabilities and high efficiency, are used in this study. Following their interaction with the detector, the high-energy (HE) and low-energy (LE) gamma rays are separated using a multi-channel analyzer (MCA) and recorded one by one parallelly (Knoll, 2010). LE and HE signals are separated and recorded as distinct arrays for all detectors and at all angles. Compton and Rayleigh scattered gamma-ray photons, as well as characteristic X-ray photons around 32 keV corresponding to the K peak of Cs-137, fall within the system's noise region. By setting the ROI (Region of Interest) on the full energy peaks (FEP), only the peaks corresponding to photoelectric interactions are recorded and separated. Figure 3 shows the acquisition and separation of the signals corresponding to high-energy and low-energy gamma photons at each angle, from the first step to the projection data transfer to the computer.

2.6 Filtered back-projection (FBP)

FBP image reconstruction method has been chosen for tomographic image formation due to the potentially large size of sinogram matrix. Iterative methods are proper when our projection data is low and normal computational devices can handle it. The attenuation profile for each angle θ along each path R of the projections is represented by Eq. (1) (TECDOC, 2008).

$$g_\theta(R_i) = \frac{1}{d} \ln\left(\frac{I_\theta^0(R_i)}{I_\theta(R_i)}\right) \tag{1}$$

where $g_\theta(R_i)$ represents the projection, d is the length passed, $I_\theta^0(R_i)$ is the intensity of the radiation recorded on the detector at angle θ in the absence of the pipeline, and $I_\theta(R_i)$ is the intensity of the gamma rays recorded on the detector at angle θ the phantom collecting will create sinogram matrix. A cross-sectional image of the item in spatial space can be obtained by backprojecting the sinogram matrix (De Chiffre et al., 2014; Yanch et al., 1992). We obtain the final image by backprojecting onto the rays' path, as per Eq. (2):

$$g_\theta(R) = \int_{(\theta,R)line} \mu(x,y)\,\mathrm{d}x\mathrm{d}y \tag{2}$$

The spatially reconstructed image is a map of the attenuation coefficients $\mu(x, y)$. In addition to altering the space (from spatial frequency to space), backprojection also greatly amplifies noise. on order to lessen the noise effect on the image, filters should be applied (Eq. (3)). Without significantly increasing the computing load during the picture reconstruction process utilizing the FBP approach, the Hamming filter exhibits good performance in noise attenuation.

where m is the maximum spatial frequency that narrows or widens the frequency range and is the spatial frequency. Equation (3) states that each row of the sinogram matrix receives a one-dimensional application of the Hamming filter (Haghighat, 2020). Through backprojecting and a two-dimensional inverse Fourier transform applied to the projections' Fourier transform, the image is recreated in spatial space.

$$\begin{aligned} F^{-1}\Big\{F\Big\{g_\theta(R)|\rho|\Big[0.54+0.46\cos\Big(\frac{\pi\rho}{\rho_m}\Big)\Big]\Big\}\Big\} = \\ = g_\theta(R) \times F^{-1}\Big\{|\rho|\Big\} \end{aligned} \tag{3}$$

As previously explained, the LE and HE signals are separated and recorded independently and simultaneously during the dual-energy process. Figure 4 illustrates the process of reconstructing the dual-energy image for each by going from the sinogram input to the spatial space image output.

2.7 Evaluation of Reconstructed Image Quality

An appropriate quantitative indicator of the accuracy of the reconstructed image in comparison to the background is the Root Mean Square Error (RMSE). Equation (4) (Prince and Links, 2006) can be used to calculate this

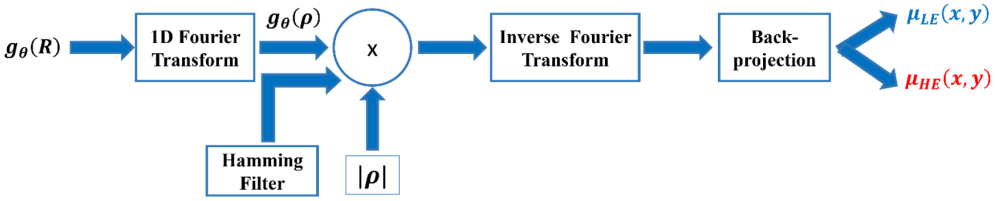

Figure 4: Image Reconstruction of DE-LNDCT process using FBP algorithm.

value:

$$RMSE = \sqrt{\frac{\sum_{j=1}^{N}(\mu_j^{reconstructed} - \mu_j^{true})^2}{N}} \tag{4}$$

where N is the number of pixels, reconstructed $\mu_j^{reconstructed}$ is the measured attenuation coefficient after reconstruction, and actual μ_j^{true} is the actual attenuation coefficient.

The contrast-to-noise ratio (CNR) is another crucial metric that may be used to assess the quality of any digital image. Equation (5) (Prince and Links, 2006) defines this parameter:

$$CNR = \frac{|S_{ROI} - S_B|}{\sigma_B} \tag{5}$$

where S_{ROI} is the average of signal of pixels within the ROI corresponding to the pipeline wall or scale area, S_B is the average signal of the background area, and σ_B represents the standard deviation of pixels in the background.

3 Results and Discussion

The validation of MC and experimental results is shown in Fig. 5. The results show very good agreement between the experimental and simulation modeling on the specific detectors.

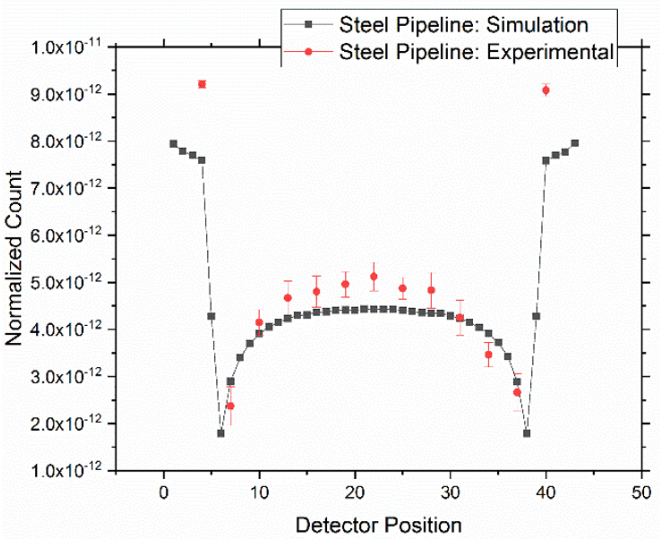

Figure 5: Monte-Carlo simulation results benchmarking with experimental results for Carbon steel test pipeline using the Cs-137 gamma ray energy.

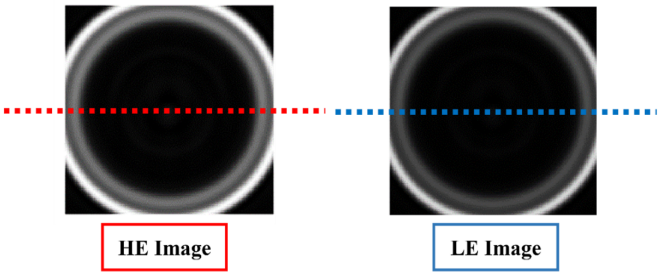

Figure 6: Reconstructed HE and LE images.

Reconstructed image by FBP is shown in the Fig. 6. The left image is high-energy image and the right one is the image reconstructed by low-energy signals.

Linear profiles along an image center were used to assess the pipelines' reconstructed images. As can be seen in Fig. 5, the red dashed line is the linear profile for HE images gray value assessment and the blue dashed line represent the linear profile across the LE image. Gray levels represent the attenuation coefficient correspond to each voxel of final image. The reconstruction of the image corresponding to high- and low-energy photons for Phantom A yielded the following results, as seen in Fig. 7, the gray level values for HE is more closely aligned with the actual value for the higher atomic number steel wall.

For materials with a lower atomic number (scale materials), the gray values are closer with the actual value for LE energy. This fact demonstrates that the cross-sectional interaction for low-energy photons is more prominent for light materials (low-Z), but for heavy materials the opposite is true.

Due to the larger signal of the photo-peak associated with high energy, the gray levels (Attenuation coefficients) in the image for the pipeline wall region are closer to the normalized actual value for the steel wall with a high atomic number. Table 3 presents quantitative measurements obtained from picture reconstruction.

According to the measured data of reconstructed image of phantom A, LE image has a higher RMS Error than the HE but the contrast-to-noise ratio of HE is better than LE image.

Table 3: RMSE and CNR of test phantom A's reconstructed image.

		RMS Error	CNR
Phantom A	LE	0.104	37.5
	HE	0.089	42.8

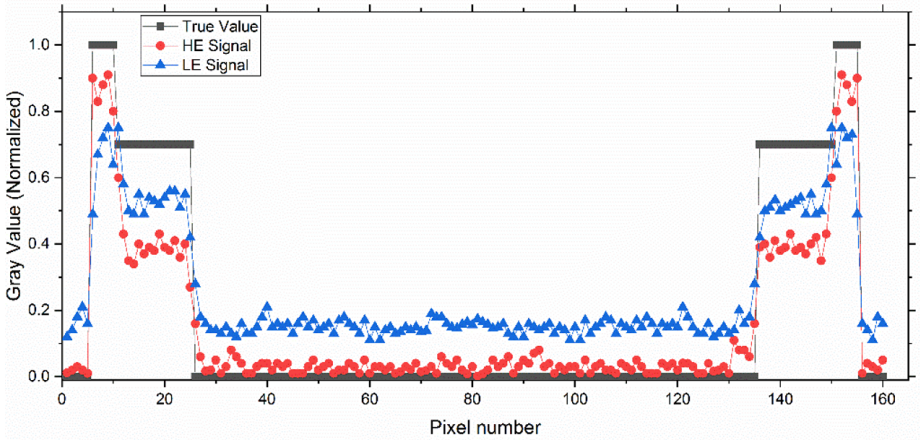

Figure 7: linear profiles of gray values obtained from images resulting from LE and HE signals of phantom A: carbon steel pipeline and anhydrite deposits.

4 Conclusions

This work used the Monte Carlo approach to conduct a feasible evaluation of the industrial design and construction of a portable pipeline tomography with limited dual-energy detectors. Originally, a computer program was used to carry out every step of the described approach, from defining the source to moving through the substance and registering in the detectors. The program receives a template file that contains the geometry definition and other pertinent information. Simultaneously, two tomographic images are reconstructed using FBP algorithm: one for high-energy (HE) and one for low-energy (LE). Gamma-ray sources of Cs-137 and Am-241 were employed for a carbon steel pipeline phantom with an anhydrite scale (phantom A) in order to implement the dual-energy approach. Following image reconstruction, the signal in the higher metal zone in HE was more desirable, whereas the signal in the lower density region in LE was closer to the genuine value. This demonstrates the dual-energy method's efficacy and correct operation in material differentiation. On the other hand, while employing more energy, the signal for the metal region is closer to the actual value. Better discriminating between heavy and light materials is demonstrated by the contrasts of the pictures and CNR in the regions of interest, particularly when the materials are adjacent. The results of this paper greatly enhance the pipeline tomography process and demonstrate that the experimental implementation and manufacturing of the DE-LNDCT equipment utilizing this Monte Carlo study is totally feasible. Future research can concentrate on optimizing the choice of LE and HE energies according to the kind of material under evaluation for additional validation, which may result in even better reconstructed images.

Conflict of Interest

The authors declare no potential conflict of interest regarding the publication of this work.

References

Ay, M. R. and Zaidi, H. (2005). Development and validation of MCNP4C-based Monte Carlo simulator for fan-and cone-beam x-ray CT. *Physics in Medicine & Biology*, 50(20):4863.

Azaman, N., Salleh, K., Abas, A., et al. (2016). Validation and application of computed radiography (CR) tangential technique for wall thickness measurement of 10 inch carbon steel pipe. In *R&D Seminar 2016: Research And Development Seminar 2016, Malaysia*.

Böttcher, B., Zsarnoczay, E., Varga-Szemes, A., et al. (2023). Dual-energy computed tomography in cardiac imaging. *Radiologic Clinics*, 61(6):995–1009.

Chung, R., Dane, B., Yeh, B. M., et al. (2023). Dual-energy computed tomography: Technological considerations. *Radiologic Clinics*.

De Chiffre, L., Carmignato, S., Kruth, J.-P., et al. (2014). Industrial applications of computed tomography. *CIRP Annals*, 63(2):655–677.

Haghighat, A. (2020). *Monte Carlo methods for particle transport*. Crc Press.

Harara, W. (2005). Evaluation of corrosion and deposit in pipes by radiography. *Development of Protocols for Corrosion and Deposits Evaluation in Pipes by Radiography*, page 85.

Hartley-Blossom, Z. J. and Digumarthy, S. R. (2023). Dual-Energy Computed Tomography Applications in Lung Cancer. *Radiologic Clinics of North America*, 61(6):987–994.

Kabir, M., Afarideh, H., Ghergherehchi, M., et al. (2024). Innovative projection acquisition algorithm for optimizing portable LNDCT in oil and gas pipeline imaging. *Nuclear Engineering and Technology*.

Kamal, M. S., Hussein, I., Mahmoud, M., et al. (2018). Oilfield scale formation and chemical removal: A review. *Journal of Petroleum Science and Engineering*, 171:127–139.

Khorsandi, M. and Feghhi, S. (2016). Gamma-ray CT as a complementary technique for structural inspection of tray-type distillation columns. *Measurement*, 78:1–8.

Kim, J., Jung, S., Moon, J., et al. (2011). Industrial gamma-ray tomographic scan method for large scale industrial plants. *Nuclear Instruments and Methods in Physics Research Section A: Accelerators, Spectrometers, Detectors and Associated Equipment*, 640(1):139–150.

Kim, J., Jung, S., Moon, J., et al. (2012a). A feasibility study on gamma-ray tomography by Monte Carlo simulation for development of portable tomographic system. *Applied Radiation and Isotopes*, 70(2):404–414.

Kim, J., Jung, S.-h., Moon, J., et al. (2012b). Development of transportable gamma-ray tomographic system for industrial application. *Nuclear Instruments and Methods in Physics Research Section A: Accelerators, Spectrometers, Detectors and Associated Equipment*, 693:203–208.

Knoll, G. F. (2010). *Radiation detection and measurement*. John Wiley & Sons.

Oliveira, D. F., Nascimento, J. R., Marinho, C. A., et al. (2015). Gamma transmission system for detection of scale in oil exploration pipelines. *Nuclear Instruments and Methods in Physics Research Section A: Accelerators, Spectrometers, Detectors and Associated Equipment*, 784:616–620.

Prasetyo, E., Pariaman, H., and Sulistijono (2020). Tangential X-ray radiography for pitting geometry analysis of outside wall of insulated steel pipes. *Russian Journal of Nondestructive Testing*, 56:249–258.

Prince, J. L. and Links, J. M. (2006). *Medical imaging signals and systems*, volume 37. Pearson Prentice Hall Upper Saddle River.

Rostron, P. (2018). Critical review of pipeline scale measurement technologies. *Indian Journal of Science and Technology*, 11(17):1–18.

Smith, E. B., Patel, L. D., and Dreizin, D. (2022). Postoperative Computed Tomography for Facial Fractures. *Neuroimaging Clinics*, 32(1):231–254.

Srinivas-Rao, S., Cao, J., Marin, D., et al. (2023). Dual-energy computed tomography to photon counting computed tomography: emerging technological innovations. *Radiologic Clinics*, 61(6):933–944.

TECDOC, I. (2008). 1589, Industrial Process Gamma Tomography, Final Report of a Coordinated Research Project 2003–2007. *International Atomic Energy Agency, Austria*.

Velo, A., Hamada, M., Carvalho, D., et al. (2017). A portable tomography system with seventy detectors and five gamma-ray sources in fan beam geometry simulated by Monte Carlo method. *Flow Measurement and Instrumentation*, 53:89–94.

Yanch, J., Dobrzeniecki, A., Ramanathan, C., et al. (1992). Physically realistic Monte Carlo simulation of source, collimator and tomographic data acquisition for emission computed tomography. *Physics in Medicine & Biology*, 37(4):853.

Zahedzadeh, M., Karambeigi, M., Roayaei, E., et al. (2014). Comprehensive management of mineral scale deposition in carbonate oil fields–A case study. *Chemical Engineering Research and Design*, 92(11):2264–2272.

Zirnhelt, J., Einav, I., and Infanzón, S. (2003). Radiographic evaluation of corrosion and deposits: An IAEA Co–ordinate Research Project. In *3rd PAN American Conference for Non-Destructive Testing-PANNDT*, volume 2.

To cite this article:

Kabir, M. , Afarideh, H. , Ghergherehchi, M. and Chai, J. (2025). Feasibility study of dual-energy limited-number-detector computed tomography of oil and gas pipelines. *Radiation Physics and Engineering*, 6(3), 27-33. doi: 10.22034/rpe.2025.490153.1257

DOI: 10.22034/rpe.2025.490153.1257

To link to this article: https://doi.org/10.22034/rpe.2025.490153.1257